Ab Initio Study on the Oxidation of NCN by OH: Prediction of the Individual and Total Rate Constants

R. S. Zhu, Hue M. T. Nguyen,[†] and M. C. Lin*

Department of Chemistry; Emory University; Atlanta, Georgia 30322

Received: July 2, 2008; Revised Manuscript Received: October 27, 2008

The mechanism for the reaction of NCN with OH has been investigated by ab initio molecular orbital and transition-state theory calculations. The potential energy surface (PES) was calculated by the highest level of the modified GAUSSIAN-2 (G2M) method, G2M(CC1). The barrierless association process of OH + NCN → OH···NCN (van der Waals, vdw) was also examined at the UCCSD(T)/6-311+G(3df,2p)//B3LYP/6-311+G(d,p) and CASPT2(13,13)/ANO-L//B3LYP/6-311+G(d,p) levels. The predicted heats of reaction for the production of H + NCNO, HNC + NO, HCN + NO, and N_2 + HOC, 7.8, −53.2, −66.9, and −67.7, respectively, are in excellent agreement with the experimental values, 8.2 ± 1.3, −52.3 ± 1.7 (or 55.7 ± 1.7), −66.3 ± 0.7, and −68.1 ± 0.7 kcal/mol. The kinetic results indicate that, in the temperature range of 300−1000 K, the formation of *trans*,*trans*-HONCN (LM2) is dominant. Over 1000 K, formation of H + NCNO is dominant, while the formation of HCN + NO becomes competitive. The rate constants for the low-energy channels given in units of cm^3 $molecule^{-1}$ s^{-1} can be represented by the following: $k_1(LM2) = 1.51 \times 10^{15} T^{-8.72} \exp(-2531/T)$ at 300−1500 K in 760 Torr N_2; $k_2(H+NCNO) = 5.54 \times 10^{-14} T^{-0.97} \exp(-3669/T)$ and $k_3(HCN+NO) = 7.82 \times 10^{-14} T^{0.44} \exp(-2013/T)$ at 300−2500 K, with the total rate constant of $k_t = 3.18 \times 10^{2} T^{-4.63} \exp(-740/T)$, 300−1000 K, and $k_t = 2.53 \times 10^{-14} T^{1.13} \exp(-489/T)$ in the temperature range of 1200−2500 K. These results are recommended for combustion modeling applications.

I. Introduction

The reaction of CH with molecular nitrogen has been predicted to be responsible for the "prompt NO" formation in the primary zone of a hydrocarbon flame.[1] In 2000, Lin and co-workers[2,3] put forth a new mechanism for the CH + N_2 reaction based on a high-level potential energy surface calculation. The reaction was shown to produce HNCN and/or H + NCN via a spin-allowed pathway, CH + N_2 → cyclic-C(H)NN- → HNCN → H + NCN; the predicted rate constant is considerably more favorable than that by the long accepted Fenimore mechanism[1] for prompt NO formation. The formation of NO can in principle result from the rapid oxidation of NCN and, to some extent, HNCN, by O, OH, and O_2 present in the primary flame zone.[2,3] Because the kinetics of NCN radical reactions are not available in the literature, we have since computationally predicted the rate constants for some key reactions involving NCN for combustion modeling applications. In our previous works, we have reported the reaction mechanisms and kinetics for the oxidation of NCN by O_2 and O.[4,5] The results show that the oxidation NCN by O_2 producing NCO + NO and CNO + NO is very slow (in the order of 10^{-15} cm^3 $molecule^{-1}$ s^{-1}) because of the high entrance and exit barriers.[4] However, the oxidation of NCN by O is very fast giving primarily CN + NO,[5] about 4−5 orders of magnitude greater than the reaction of NCN with O_2.

In this work, the oxidation reaction of NCN by OH has been investigated. We have attempted to map out a detailed potential energy surface (PES) for the system and calculated the rate constants for the reaction taking place along the low-lying energy pathways. The results of this study providing the individual and total rate constants are presented herein.

II. Computational Methods

The geometries of the reactants, intermediates, transition states, and products for the NCN + OH reaction were optimized at the hybrid density functional UB3LYP/6-311+G (3df,2p) level of theory, i.e., Becke's three-parameter nonlocal-exchange functional [6−8] with the nonlocal correlation functional of Lee, Yang, and Parr.[9] The vibrational frequencies, calculated at this level, were used for characterization of stationary points' zero-point energy (ZPE) corrections. All the stationary points were identified for local minima (with the number of imaginary frequencies equal to zero) and transition states (each with one imaginary frequency). Intrinsic reaction coordinate (IRC) calculations[10] were performed to confirm the connection between a transition state and designated intermediate. To obtain reliable energies, the PES was calculated using the highest scheme of the modified GAUSSIAN-2 (G2M) method, G2M(CC1)[11] which employed a series of calculations with the B3LYP optimized geometry to approximate the CCSD(T)/6-311+G(3df,2p) level of theory, including a "higher level correction" based on the number of paired and unpaired electrons. In the NCN + O_2[4] and NCN + O[5] systems, the G2M(CC1) method can better reproduce the experimental heats of reaction than the CASPT2 or the MRCI + Q can, and the dissociation energies for NCN−O and NC−NO obtained at the G2M (CC1) level are very close to those obtained by the MRCI + Q level, the deviations are only 1.1 and 0.5 kcal/mol, respectively. Therefore, in this calculation, the G2M (CC1) method is mainly used for the refined energies.

To treat the multireference effect on the barrierless association process, the single point energies along the minimum energy

---

* Corresponding author; email chemmcl@emory.edu.

[†] Present address: Department of Chemistry, Hanoi National University of Education, Hanoi, Vietnam, 644410.

10.1021/jp805821x CCC: $40.75

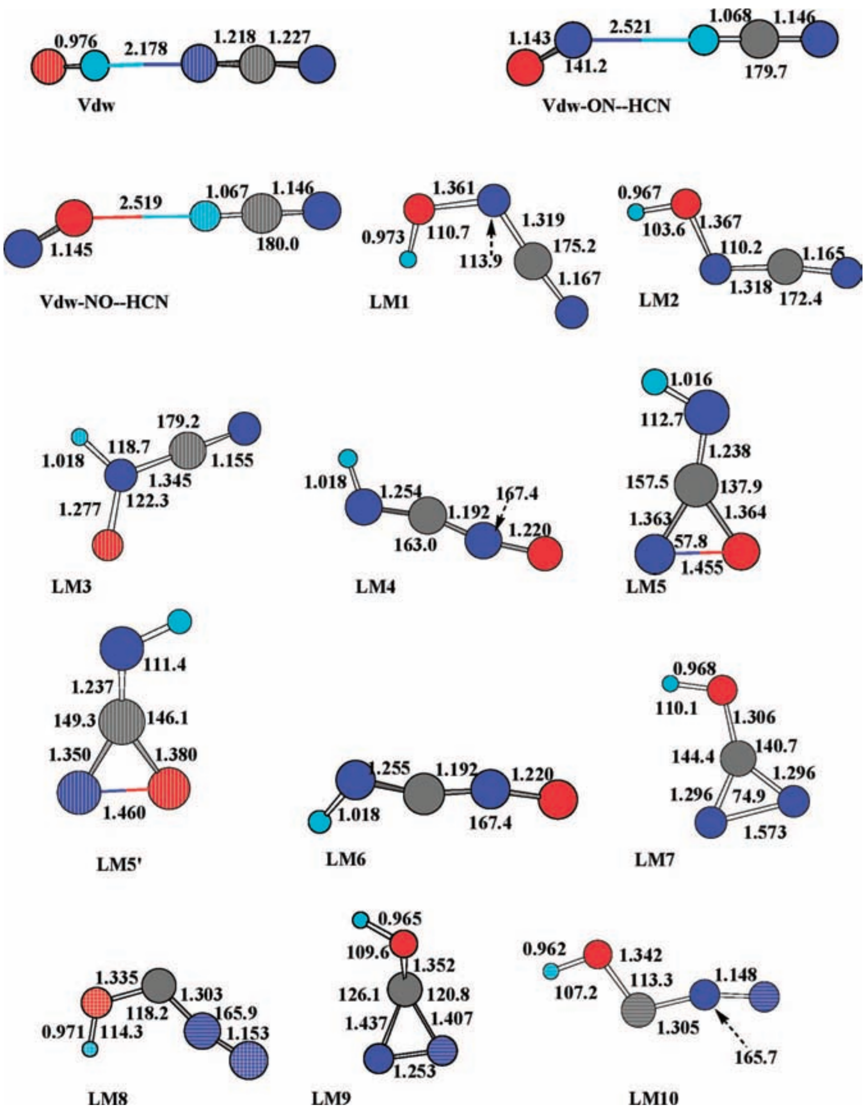

Figure 1. Optimized geometries of the intermediates for the reaction of NCN + OH at the B3LYP/6-311+G(3df,2p) level. The bond lengths are given in angstroms and angles in degrees.

path (MEP) of OH + NCN → OH···NCN (van der Waals, vdw) at the CASPT2(13,13)/ANO-L level were calculated by MOLCAS program,[12] where, (13,13) represents 13 electrons in 13 active orbitals. The 13 electrons contain 3 from OH and 10 from NCN; similarly, 3 orbitals from the OH and 10 orbitals from the NCN radical. The other molecular orbital calculations were done using the Gaussian 03 program.[13] For prediction of rate constants, we have employed the Variflex[14] and ChemRate codes[15] to couple all low-lying reaction channels including isomerization processes by solving the T- and P-dependent master equation.

III. Results and Discussion

A. Potential Energy Surface and Reaction Mechanism. The optimized geometries of the intermediates and transition states at the B3LYP/6-311+G(3df,2p) level are shown in Figures 1 and 2, respectively. The potential energy diagram obtained at the G2M(CC1) level is presented in Figure 3. Figure 4 shows the low-lying energy channels used in the rate constant calculations. The vibrational frequencies and rotational constants of all species are summarized in the Supporting Information (SI-1).

H + NCNO Formation. The interaction between the hydrogen atom of the OH radical and one of the N atoms in NCN forms a nearly linear prereaction van der Waals complex (OH···NCN) lying below the reactants by 5.2 kcal/mol. The complex can readily transfer to more stable *cis*,*trans*-HONCN (LM1) via a loose transition state (vdw-TS) with only 0.4 kcal/mol barrier height. By rotation of the OH group around the O−N bond, the *cis*,*trans*-HONCN can readily isomerize to *trans*,*trans*-HONCN (LM2) via TS1 with only 7.8 kcal/mol barrier above the LM1. LM1 and LM2 lie below the reactants by 49.9 and 53.3 kcal/mol, respectively; both intermediates can directly decompose to H + NCNO with 7.8 kcal/mol endothermicity. The pathways to form H + NCNO can be represented by Scheme 1.

HCN + NO Formation. To help understand the low-energy reaction pathways for the formation of HCN + NO, the energy diagram was simplified and illustrated by Scheme 2. There are two paths to produce HCN + NO: the first one takes place via LM1, which dissociates to form a loose complex (vdw-NO···HCN) via TS2 with a high barrier of 22.7 kcal/mol above the reactants. It should be pointed out that for the IRC analysis of TS2, if the default step size value (0.1 amu$^{1/2}$·bohr) is used or the value is over 0.02, the IRC analysis cannot be smoothly carried out for the forward direction. The IRC results were plotted in the Supporting Information (SI-2), which shows that, for the forward direction, the H atom migrates from O to the C

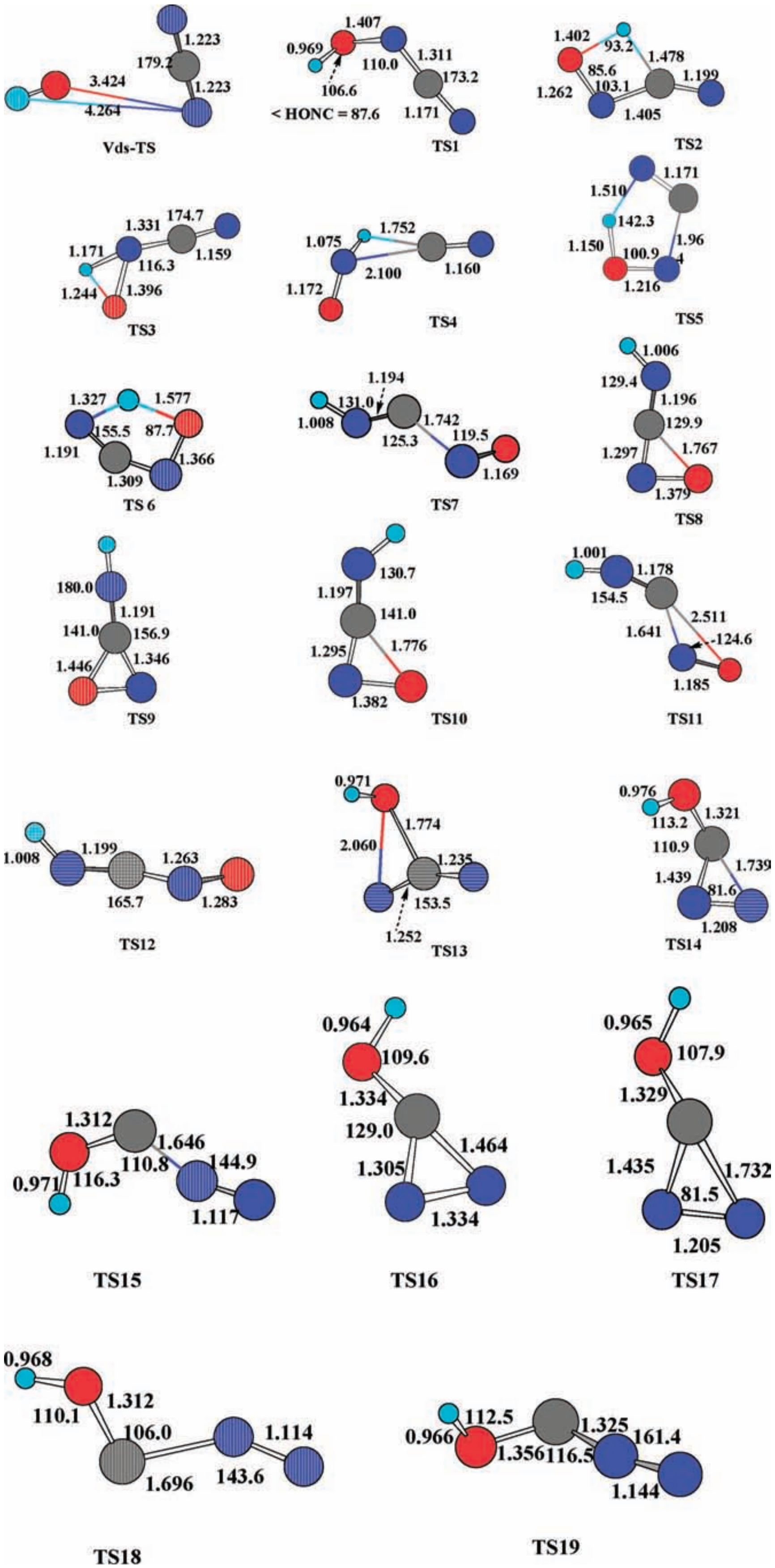

Figure 2. Optimized geometries of the transition states involved in the reaction of NCN + OH at the B3LYP/6-311+G(3df,2p) level. The bond lengths are given in angstroms and angles in degrees.

atom, simultaneously, the C−N bond is lengthened from 1.405 Å in TS2 to 2.358 Å in the final structure. When we used the final point as the initial input to optimize, a loose complex (vdw-NO···HCN) was located at 0.7 kcal/mol below the final

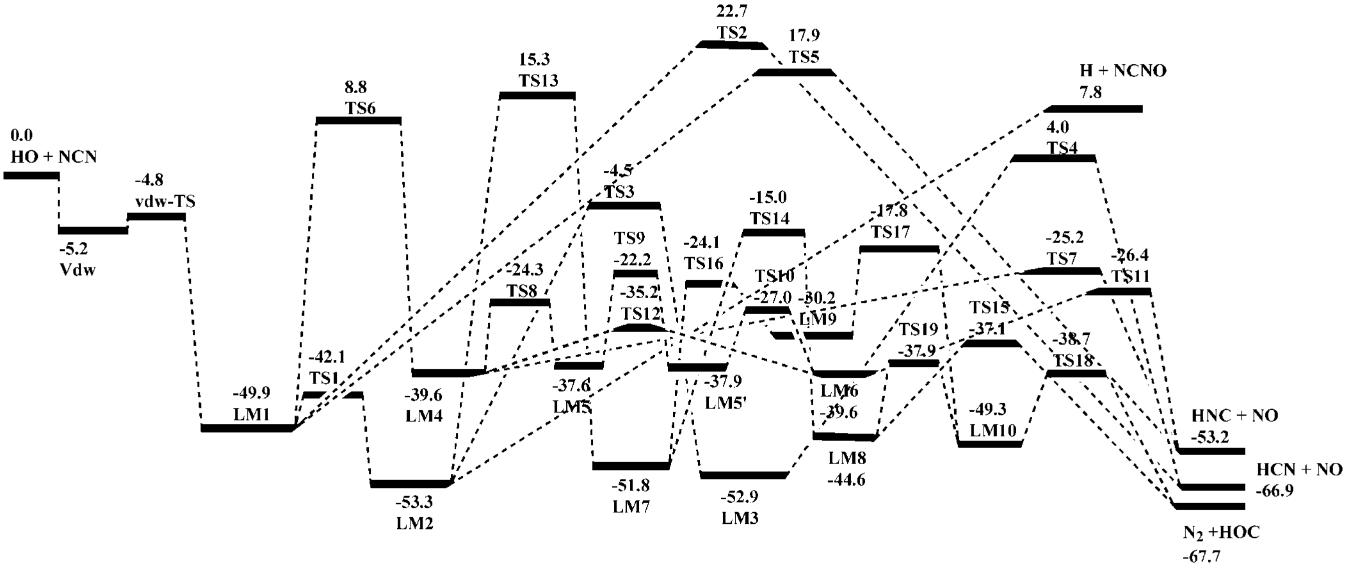

Figure 3. Energy diagram (kcal/mol.) for the NCN−OH system, computed at the G2M(CC1) level.

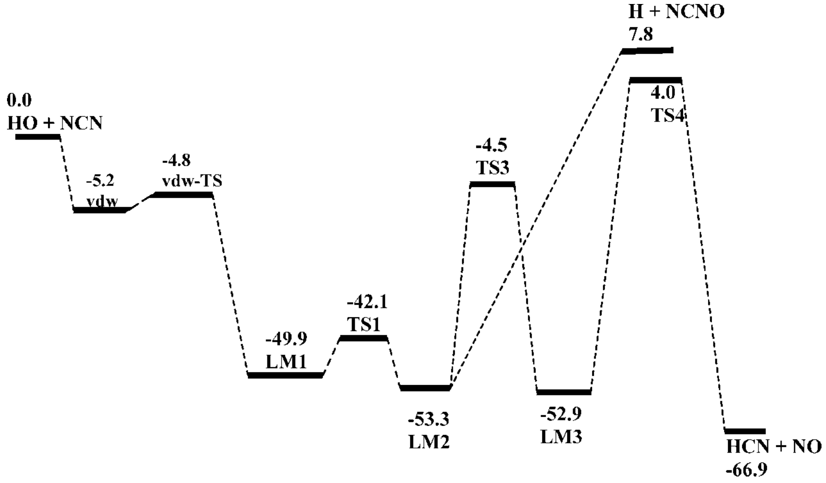

Figure 4. Low-lying energy diagram (kcal/mol) used in the rate constant calculations, computed at the G2M(CC1) level.

SCHEME 1

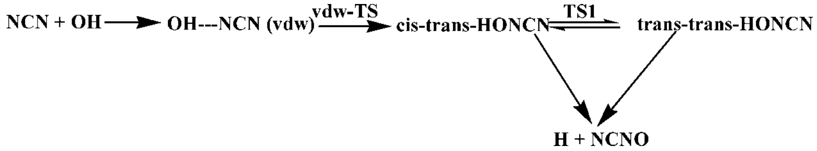

SCHEME 2

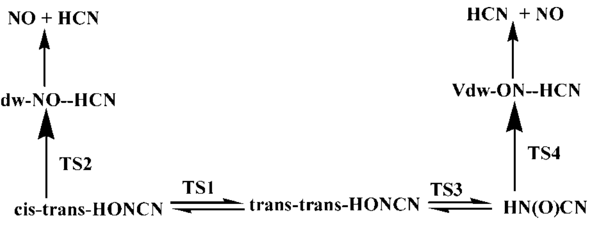

products HCN + NO. The second pathway occurs by H-atom migration from *trans*,*trans*-HONCN to the neighboring N atom to form HN(O)CN (LM3) via TS3. LM3 is lower than *cis*,*trans*-HONCN by 3 kcal/mol but slightly higher than *trans*,*trans*-HONCN by 0.4 kcal/mol. TS3 is 48.8 kcal/mol above the *trans*,*tans*-HONCN intermediate. LM3 transforms to a loose complex (vdw-ON···HCN) via TS4 with a barrier height of 56.9 kcal/mol and the vdw-ON···HCN dissociates to the products HCN + NO. The loose complex lies 1.1 kcal/mol below the products.

SCHEME 3

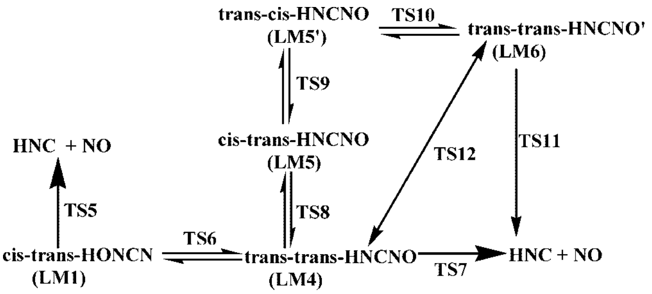

HNC + NO Formation. As shown in Scheme 3, in *cis*,*trans*-HONCN, the H atom can migrate from OH group to the terminal N atom and simultaneously break the N−C bond to produce HNC + NO via a five-member-ring transition state TS5 lying

SCHEME 4

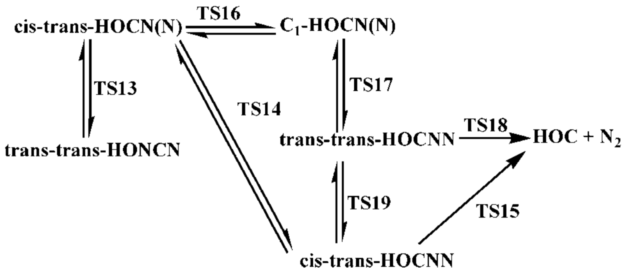

TABLE 1: Comparison of the Experimental Heats of Reaction (kcal/mol) and the Values Calculated at the G2M(CC1) Level

reactants	products	calculated	experimental[a]
NCN + OH	H + NCNO	7.8	8.2 ± 1.3
NCN + OH	HNC + NO	−53.2	−52.3 ± 1.7 to −55.7
NCN + OH	HCN + NO	−66.9	−66.3 ± 0.7
NCN + OH	N_2 + HOC	−67.7	−68.1 ± 0.7

[a] The experimental values are derived from the known experimental heats of formation as mentioned in the text.

67.8 kcal/mol above LM1 (or 17.9 kcal/mol above the reactants). The N−C bond in TS5 is lengthened from 1.311 Å in LM1 to 1.964 Å in TS5. The alternative low-energy path is the isomerization of *cis*,*trans*-HONCN to *trans*,*trans*-HNCNO (LM4) via TS6 with an 8.8 kcal/mol barrier above the reactants; the LM4 intermediate further dissociates to HNC + NO via TS7 with a 14.4 kcal/mol barrier. Meanwhile, LM4 can also isomerize to *cis*,*trans*-HNCNO (LM5) via TS8 with a 15.3 kcal/mol barrier, and then LM5 isomerizes to LM5′ via TS9 with 16.2 kcal/mol barrier; breaking the C−O bond in LM5′ via TS10 with 10.9 kcal/mol barrier forms a chain *trans*,*trans*-HNCNO′ (LM6) which further dissociates to the products HNC + NO via TS11 costing 13.2 kcal/mol energy. LM4, LM6, LM5, and LM5′ appear to be optical isomers. LM4, LM5, LM5′, and LM6 lie below the reactants by 39.6, 37.6, 37.9, and 39.6 kcal/mol, respectively. The isomerization transition state (TS12) between LM4 and LM6 is also located; its energy is only 4.4 kcal/mol higher than that of the former.

N_2 + HOC Formation. As shown in Scheme 4, the LM2 intermediate can first isomerize to *cis*,*trans*-HOCN(N) (LM7) via TS13 with a rather high 68.8 kcal/mol barrier; LM7 can isomerize to an open-chain *cis*,*trans*-HOCNN (LM8) via TS14, to be followed by the fragmentation of LM8 to HOC + N_2 by breaking the C−N bond via TS15. In TS15, the breaking C−N bond is 0.343 Å longer than that in LM8. Second, the *cis*,*trans*-HOCN(N) intermediate can undergo isomerization to another C_1 symmetry isomer C_1−HOCN(N) (LM9) via TS16 with a 27.7 kcal/mol barrier. C_1-HOCN(N) isomerizes to *trans*,*trans*-HOCNN (LM10) via TS17 with a 12.4 kcal/mol barrier. *trans*,*trans*-HOCNN decomposes readily to HOC + N_2 via TS18 with a 10.6 kcal/mol barrier. Comparing these two pathways, one finds that, relatively, the *cis*,*trans*-HOCNN decomposes more readily than the *trans*,*trans*-HOCNN isomer. However, since the formation of the intermediate LM7 needs to overcome a high-energy transition state (TS13), these two product channels are controlled mainly by TS13; therefore, the formation of N_2 is expected to be kinetically unfavorable.

B. Heats of Reaction for Different Channels. As shown in Table 1, the heats of reaction for the production of H + NCNO, HNC + NO, HCN + NO, and N_2 + HOC are predicted to be 7.8, −53.2, −66.9, and −67.7, respectively; they are in excellent agreement with the experimental values, 8.2 ± 1.3, −52.3 ± 1.7 (or 55.7 ± 1.7), −66.3 ± 0.7, and −68.1 ± 0.7 kcal/mol. The experimental values are derived from the known experimental heats of formation at 0 K: NCN (111.3 ± 0.7 kcal/mol),[16] OH (8.86 ± 0.007 kcal/mol),[17] H (51.63 ± 0.0014),[18] NCNO (76.7 kcal/mol),[18] NO (21.46 ± 0.04 kcal/mol),[18] HCN (32.4 kcal/mol),[18] HNC (43 ± 1.0 and 46.4 kcal/mol), [19,20] and CN (104.1 ± 0.5 kcal/mol).[21] The heat of formation of HOC (52.1 kcal/mol) was calculated at the CCSD(T)/cc-pv5z level.[22] The heat of formation for NCNO is determined by the experimental dissociation energy (48.85 ± 0.03 kcal/mol)[23] and the heats of formation of CN and NO mentioned above. In the similar system of NCN + O_2,[4] we compared the exothermicity for the formation NCO + NO at the G2M(CC1), CASPT3, and MRCI + Q levels, the results show that, at the G2M(CC1) level, the calculated value of 60.0 kcal/mol is in good agreement with the experimental one, −59.4 ± 1.7 kcal/mol; however, the values at the CASPT3 and MRCI + Q are around 9.0 and 5.0 kcal/mol lower than the experimental value. The deviations may arise from the limited active space and limited active electrons. On the basis of these comparisons, the energies at the G2M(CC1) level are used for the following kinetic treatments.

C. VTST Calculations for the Association/Decomposition Processes. Our test shows that the structures of *cis*,*trans*-HONCN and *trans*,*trans*-HONCN obtained at the B3LYP/6-311+G(3df,2p) level are close to those obtained at the B3LYP/6-311+G(d,p) level; the maximum deviation of the bond length and bond angles are only 0.02 Å and 0.5°, respectively. Meanwhile, the G2M(CC1) energies based on the structures obtained by the above basis sets have less than 0.1 kcal/mol difference. Therefore, the variational association/dissociation curves were calculated using the 6-311+G(d,p) basis set. For the barrierless association process of HO + NCN → OH···NCN (vdw), the potential energy curve was computed from the stable OH···NCN (vdw) to cover the H−N bond with separation from 2.189 to 4.189 Å, with an interval step size of 0.2 Å; other geometric parameters were fully optimized without symmetry constraint. For the decomposition of H−ONCN, the H−O bond was separated from 0.967 to 4.267 Å.

To illustrate the method effect on the MEP, we take the process of OH + NCN → OH···NCN (vdw) as an example, on the basis of the structures obtained at the UB3LYP/6-311+G(d,p) level, the single point energies along the MEP were also refined at the UCCSD(T)/6-311+G(3df,2p) and CASPT2 (13,13)/ANO-L levels, respectively. The MEPs predicted by the three methods are plotted as shown in the Supporting Information (SI-3). As one can see, the relative energies along the MEP obtained at the UCCSD(T)/6-311+G(3df,2p) and UB3LYP/6-311+G** levels match very well within the varitional distance range, while, below 3.5 Å, the curve at the CASPT2 level has some deviation compared with those by the former two methods. The effect of this deviation on the rate will be examined in the rate constant calculation part.

IV. Rate Constant Calculations

Variational TST and RRKM calculations have been carried out for the low-lying energy channels shown in Scheme 5 (the PES is shown in Figure 4).

In Scheme 5, ∗ indicates an activated molecule and M is the third body (N_2 in this work). On account of the absence of a well-defined transition state for the initial association process HO + NCN → OH···NCN (vdw), the potential function was computed variationally as discussed above. The Morse potential function $E(R) = D_e[1 - e^{-\beta(R-R_e)}]^2$, was employed to approximate the minimum energy path in our rate constant

SCHEME 5

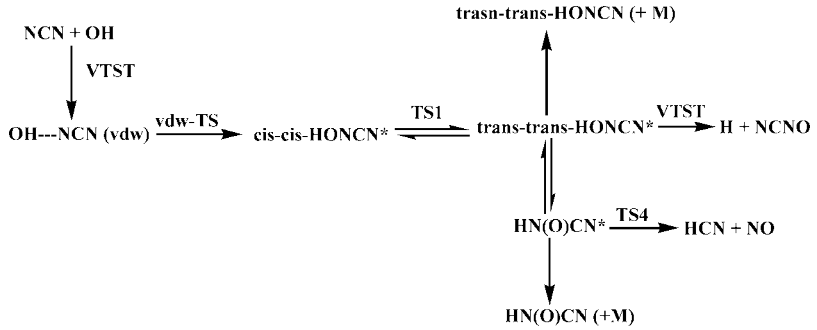

calculation. In the above equation, R is the reaction coordinate (i.e., the distance between the two bonding atoms; the H−N bond in this work), D_e is the bond energy excluding zero-point energy, and R_e is the equilibrium value of R. The potential energies at the UB3LYP/6-311+G**, the CCSD(T)/6-311+G(3df,2p)//B3LYP/6-311+G** and CASPT2 (13,13)/ANO-L//B3LYP/6-311+G** levels could be fitted reasonably to the Morse potential function with the parameters of $\beta = 1.550$ and 1.560 and 1.396 Å^{-1}, respectively. For the tight transition states, the numbers of states were evaluated according to the rigid-rotor harmonic oscillator. To calculate the collision rate between the complex (HO−NCN) and the bath gas (N_2), the Lennard-Jones parameters for the HO−NCN−N_2 pair, $\sigma = 3.9$ Å and $\varepsilon = 205$ K, were assumed to be the same as those of NCNO−N_2, taken from ref 24. The pressure dependence of rate constants was predicted by the exponential-down model in the solution of the master equation using $\langle \Delta E \rangle_{\rm down} = 200$ cm^{-1}, ignoring a possible small temperature dependence of the averaged energy-transfer step size.[25−28]

Our test shows that LM1 can 100% transfer to LM2 since the forward barrier is 32.3 kcal/mol lower than the reverse one (see Figure 4); therefore, in the calculation with Variflex,[14] TS1 was ignored; TS4 was taken as the rate-controlling transition state for the formation of HCN + NO since TS3 is 8.5 kcal/mol lower than TS4.

On the basis of our previous studies,[29−31] for the type of reactions involved in a molecular complex with a shallow well, the effects of multiple reflections[32,33] among the reactants (HO + NCN, 0.0), the well (vdw, −5.2 kcal/mol), and its exit transition state (vdw-TS, −4.8 kcal/mol) are important. For this reaction, the total rate constant in 760 Torr N_2 with the multiple reflections at 300 K is a factor of 2 lower than that without reflections. Over 1200 K, the deviation is less than 3%, as shown in the Supporting Information (SI-4). Apparently, the multiple reflections at low temperatures for this system are significant. In Figure 5, only the rate constants in 760 Torr N_2 with multiple reflections are plotted.

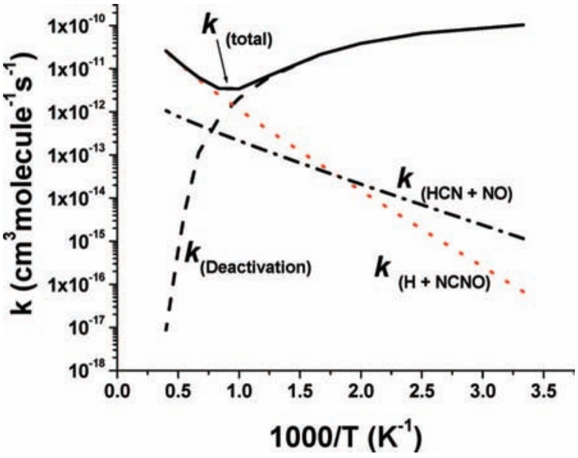

Figure 5. Predicted total and individual rate constants (in 760 Torr N_2) for the low-lying energy channels as shown in the legend.

The results indicate that, in the temperature range of 300−1000 K, the deactivation of LM2 is dominant. It should be mentioned that the deactivation of LM3 was tested using Chemrate,[15] including multiwell coupling in the calculation; formation of LM3 (HN(O)CN) is 3−31% in the temperature range of 300−800 K. The results imply that, at low temperatures, LM2 and LM3 can be stably formed from NCN + OH, which need to be experimentally confirmed. Over 1000 K, formation of H + NCNO becomes dominant and the production of HCN + NO is competitive. From 1000 to 2500 K, the NO formation rate constants lie within 2.14×10^{-13} to 1.07×10^{-12} cm^3 molecule^{-1} s^{-1}, which are apparently lower than those from the NCN + O system[5] ((1.07−1.42) × 10^{-10} cm^3 molecule^{-1} s^{-1} in the temperature range of 298−2500 K). In the NCN + O_2 system,[4] the formation of NO is not favorable; its rate lies within 1.7×10^{-18} to 2.8×10^{-15} cm^3 molecule $^{-1}$ s^{-1} in the same temperature range of 1000−2500 K.

The individual rate constants for the deactivation and the formation of H + NCNO and HCN + NO in 760 Torr N_2 in units of cm^3 molecule^{-1} s^{-1} can be expressed by

$$k_1(\text{deactivation}) = 1.51\times 10^{15}T^{-8.72}\exp(-2531/T), \quad 300-1500\ \text{K}$$

$$k_2(\text{H+NCNO}) = 5.54\times 10^{-14}T^{-0.97}\exp(-3669/T), \quad 300-2500\ \text{K}$$

$$k_3(\text{HCN+NO}) = 7.82\times 10^{-14}T^{0.44}\exp(-2013/T), \quad 300-2500\ \text{K}$$

with the following total rate constants: $k_t = 3.18 \times 10\ {}^{2}T^{-4.63}$ exp(−740/T), 300−1000 K, and $k_t = 2.53 \times 10\ {}^{-14}T^{1.13}$ exp(−489/T), 1200−2500 K.

To investigate the predicted uncertainty arising from the MEP calculated by different methods, the high-pressure-limit rate constant with the MEP calculated by CASPT2 method was examined. The results show that at 300 K, the high-pressure-limit rate increases by 4%, over 1200 K, the difference is less than 1%, compared with those based on the MEP obtained by the B3LYP method. The high-pressure-limit rates are displayed in Supprting Information SI-5.

V. Conclusion

The potential energy surface and the mechanism for the oxidation of NCN by OH have been computed at the G2M(CC1) level of theory, and the rate constants for the low-lying energy channels have been predicted. Three van der Waals complexes OH···NCN, ON···HCO, and NO···HCO and 10 stable HONCN isomers were located; the most stable one is the *trans*,*trans*-HONCN with 53.5 kcal/mol energy below the reactants, the least stable one is HOC(N)N with C_1 symmetry, lying 30.2 kcal/mol below the reactants. Kinetics results show that oxidation of NCN by OH producing *trans*,*trans*-HONCN is dominant below 1000 K; over 1000 K, formation of H + NCNO becomes dominant and the production of HCN + NO becomes competitive. This reaction is faster than the oxidation reaction of NCN by O_2 but slower than the NCN + O reaction. The equations for the individual and total rate constants are given; the results are recommended for combustion modeling applications.

Acknowledgment. This work is sponsored in part by the Office of Naval Research under Contract No. N00014-02-1-0133 and in part by the Basic Energy Sciences, Department of Energy, under Grant No. DE-FG-97ER14784. M.C.L. is grateful to the National Science Council of Taiwan for a Distinguished Visiting Professorship at the National Chiao Tung University, Hsinchu, Taiwan. We would like to thank Professor Minh Tho Nguyen, University of Leuven, Belgium, for kind assistance with the CASPT2 computations.

Supporting Information Available: Tables giving rotational constants and vibrational frequencies and high-pressure-limit rate constants and figures showing IRC results for TS2, relative energies along the minimum energy potential curves for OH + NCN → OH−NCN at different levels, and predicted temperature-dependent total rate constant with/without multiple-reflection. This material is available free of charge via the Internet at http://pubs.acs.org.

References and Notes

(1) Fenimore, C. P. *Symp. (Int.) Combust. Proc.* **1971**, *13*, 373.

(2) Moskaleva, L. V.; Xia, W. S.; Lin, M. C. *Chem. Phys. Lett.* **2000**, *331*, 269.

(3) Moskaleva, L. V.; Lin, M. C. *Proc. Combust. Inst.* **2000**, *28*, 2393.

(4) Zhu, R. S.; Lin, M. C. *Int. J. Chem. Kinet.* **2005**, *37*, 593.

(5) Zhu, R. S.; Lin, M. C. *J. Phys. Chem. A* **2007**, *111*, 6766.

(6) Becke, A. D. *J. Chem. Phys.* **1993**, *98*, 5648.

(7) Becke, A. D. *J. Chem. Phys.* **1992**, *96*, 2155.

(8) Becke, A. D. *J. Chem. Phys.* **1992**, *97*, 9173.

(9) Lee, C.; Yang, W.; Parr, R. G. *Phys. Rev.* **1988**, *B37*, 785.

(10) Gonzalez, C.; Schlegel, H. B. *J. Phys. Chem.* **1989**, *90*, 2154.

(11) Mebel, A. M.; Morokuma, K.; Lin, M. C. *J. Chem. Phys.* **1995**, *103*, 7414.

(12) Anderson, K. et al. MOLCAS, Version 7.0; Lund University: Lund, Sweden, 2007.

(13) Frisch, M. J.; Trucks, G. W.; Head-Gordon, M.; Gill, P. M. W.; Wong, M. W.; Foresman, J. B.; Johnson, B. G.; Schlegel, H. B.; Robb, M. A.; Replogle, E. S.; Gomperts, T.; Andres, J. L.; Raghavachari, K.; Binkley, J. S.; Gonzales, C.; Martin,R. L.; Fox, D. J.; DeFrees, D. J.; Baker, J.; Stewart, J. J. P.; Pople, J. A. *Gaussian 03*, Revision D. 01; Gaussian: Pittsburgh, PA, 2003.

(14) Klippenstein, S. J.; Wagner, A. F.; Dunbar, R. C.; Wardlaw, D. M. Robertson, S. H. *VARIFLEX*, Version 1.00, Argonne National Laboratory, Argonne, IL, 1999.

(15) Mokrushin, V.; Bedanov, V.; Tsang, W.; Zachariah, M. R.; Knyazev, V. D. *ChemRate*, Version 1.19; National Institute of Standards and Technology: Gaithersburg, MD, 2002.

(16) Bise, R. T.; Choi, H.; Neumark, D. M. *J. Chem. Phys.* **1999**, *111*, 4923.

(17) Ruscic, B.; Boggs, J. E.; Burcat, A.; Csaszar, A. G.; Demaison, J.; Janoschek, R.; Martin, J. M. L.; Morton, M. L.; Rossi, M. J.; Stanton, J. F.; Szalay, P. G.; Westmoreland, P. R.; Zabel, F.; Berces, T. *J. Phys. Chem. Ref. Data* **2005**, *34*, 573.

(18) Chase, M. W., Jr. *NIST-JANAF Thermochemical Tables*, 4th ed.; American Chemical Society: Washington, D.C.; American Institute of Physics for the National Institute of Standards and Technology: Woodbury: New York, 1998.

(19) Hansel, A.; Scheiring, Ch.; Glantschnig, M.; Lindinger, W.; Ferguson, E. E. *J. Chem. Phys.* **1998**, *109*, 1748.

(20) Maricq, M. M.; Smith, M. A.; Simpson, C. J. S. M.; Ellison, G. B. *J. Chem. Phys.* **1981**, *74*, 6154.

(21) Huang, Y. H.; Barts, S. A.; Halpern, J. B. *J. Phys. Chem.* **1992**, *96*, 425.

(22) Marenich, A. V.; Boggs, J. E. *J. Phys. Chem. A* **2003**, *107*, 2343.

(23) Nadler, I.; Reisler, H.; Noble, M.; Wittig, C. *Chem. Phys. Lett.* **1984**, *108*, 108.

(24) Klippenstein, S. J.; Khundkar, L. R.; Zewail, A. H.; Marcus, R. A. *J. Chem. Phys.* **1988**, *89*, 4761.

(25) Golden, D. M.; Smith, G. P.; McEwen, A. B.; Yu, C. L.; Eiteneer, B.; Frenklach, M.; Vaghjiani, G. L.; Ravishankara, A. R.; Tully, F. P. *J. Phys. Chem.* **1998**, *102*, 8598.

(26) Zhu, R. S.; Diau, E. G. W.; Lin, M. C.; Mebel, A. M. *J. Phys. Chem.* **2001**, *105*, 11249.

(27) Zhu, R. S.; Lin, M. C. *ChemPhysChem.* **2004**, *5*, 1864.

(28) Zhu, R. S.; Lin, M. C. *ChemPhysChem.* **2005**, *6*, 1514.

(29) Zhu, R. S.; Lin, M. C. *J. Phys. Chem. A* **2001**, *105*, 6243.

(30) Zhu, R. S.; Xu, Z. F.; Lin, M. C. *J. Chem. Phys.* **2004**, *120*, 6566.

(31) Zhu, R. S.; Lin, M. C. *Chem. Phys. Lett.* **2005**, *408*, 25.

(32) Hirschfelder, J. O.; Wigner, E. *J. Chem. Phys.* **1939**, *7*, 616.

(33) Miller, W. H. *J. Chem. Phys.* **1976**, *65*, 2216.

JP805821X